DENOISING METHOD FOR PARTIAL DISCHARGE SIGNAL BASED ON IMPROVED VARIATIONAL MODE DECOMPOSITION ALGORITHM

Xiaowei WANG[1]*, Zuowei PAN[1], Yan LI[1], Haiting YANG[1], Ning WANG[1], Guoliang SUN[1]

To overcome the detrimental effects of noise contamination on partial discharge signal detection, a novel denoising algorithm was proposed. This algorithm integrates the dung beetle optimization algorithm guided by improved sine (MSADBO) with Variational Mode Decomposition (VMD), and Wavelet Packet Denoising. The primary objective was to extract clean partial discharge signals by minimizing envelope entropy, serving as the fitness function. Optimal parameters for VMD, the key parameters—specifically the quantity of decomposition modes (K) and the penalty coefficient (α)—were optimized through MSADBO. These settings enabled the breakdown of distorted signals into multiple Intrinsic Mode Functions (IMFs), effectively isolating meaningful components from the noise. To distinguish between pure and noisy signals, the Pearson correlation coefficient (R) was utilized. Noisy components were subsequently removed, leaving behind the pure signals. These signals underwent reconstruction and denoising via the Wavelet Packet Denoising algorithm, resulting in a final noise-reduced signal. Compared to traditional methods EMD and VMD, this novel approach demonstrated enhanced noise suppression capabilities, highlighting its effectiveness in improving signal clarity and quality. The valid information in the original partial discharge signal were retained and validity of the proposed algorithm was verified.

Keywords: Partial Discharge; Variational mode Decomposition; The Dung Beetle Optimization Algorithm Guided by Improved Sine Algorithm; Wavelet Packet Denoising; Noise Reduction

1. Introduction

Partial discharge (PD) detection is a kind of crucial and popular method for evaluating the insulation state of electrical equipment [1,2]. Partial discharge signals were interfered by various noise signals in practical partial discharge detection scenarios. The noises included pulse-type noises, narrowband noises, and broadband noises, etc. [3,4]. True partial discharge signals were difficult to extract due to being covered by noise, which brought inconvenience to the daily maintenance and fault detection of electrical equipment [5,6]. As a result, it was

[1] Inner Mongolia Jingneng Kangbashi Thermal Power Co., Ltd, Inner Mongolia, China
*Corresponding author: Xiaowei Wang, e-mail: wxwei25@126.com

essential to minimize partial discharge signal noise and emphasize the signals' inherent qualities.

With the continuous evolution of power systems, the issue of signal interference has become increasingly prominent, driving the development of various noise reduction algorithms. In 1998, Huang and colleagues introduced an innovative adaptive signal processing technique grounded in mode decomposition principles, it was EMD (Empirical Mode Decomposition) algorithm [7]. The base functions do not need to be set in advance and any signal could be decomposed based on EMD algorithm, and the EMD algorithm had very good adaptability [8,9]. The Grey Wolf algorithm optimizes the EMD algorithm and the vector machine classification model was proposed by Fanxing Zeng et al. in 2021. The findings demonstrated that, in comparison to a Support Vector Machine optimized using a genetic algorithm (GA-SVM), multi-layer Perceptron (MLP), and K-nearest Neighbor Classifier (kNN), GMO-SVM could more reliably identify the type of local discharge source [10]. Ragavesh Dhandapani introduced a noise reduction technique for partial discharge signals using adaptive decomposition, entropy analysis, and group sparse total variation in 2021. By integrating the EMD and VMD algorithms, the proposed denoising approach demonstrated strong effectiveness in suppressing noise within partial discharge signals [11]. There were problems of modal aliasing and endpoint effects in the processing based on EMD algorithm, so noises could not be effectively removed [12,13]. In 2014, Dragomiretskiy et al. presented Variational Mode Decomposition (VMD). The VMD algorithm had a solid theoretical foundation and overcome the phenomenon of mode aliasing [14]. The signal components extracted through the VMD algorithm were capable of accurately representing the signal characteristics across multiple scales [15,16]. In 2023, Zhipeng Lei and colleagues proposed a noise reduction technique that integrates SVD combined with VMD in partial discharge (PD) signals from high-voltage equipment. These results showed that the filtered PD signal exhibited strong noise reduction, high SNR (Signal-to-Noise Ratio) and NCC (Normalized Correlation Coefficient), minimal MSE (Mean-Square Error), and preserved waveform integrity [17]. The experimental outcomes demonstrated that the WVNW (Transformer partial discharge based on the Whale VMD algorithm combined with adaptive filtering and wavelet thresholding) approach was highly effective in mitigating noise interference while retaining a large number of characteristics of partial discharge signals, restored the original discharge signal waveform, and had a high waveform similarity [18]. However, the K value of the modal decomposition number needed to be set manually, which was prone to issues related to excessive decomposition and insufficient decomposition [19]. In this work, the study report mentioned above served as the basis for the proposal of an enhanced VMD algorithm. The ideal values for the penalty parameter α and the number of breakdown modes K in the VMD were obtained. MSADBO algorithm

was used to generate the decomposition method, which guaranteed the highest level of decomposition accuracy and prevented the issue of inadequate precision brought on by the experience-based parameter selection. Each Pearson correlation coefficients of IMF (Intrinsic Mode Function) were computed using the noisy partial discharge signal, and the noisy components were removed. The remaining components were reconstructed, subsequently, the reconstructed signal underwent noise reduction using the wavelet packet algorithm and finally the denoised signal was obtained. The noise suppression ratios obtained using the proposed method, along with those from the EMD and VMD algorithms, were compared and analyzed. In contrast to the VMD and EMD algorithms, the proposed algorithm demonstrated an improved noise suppression ratio. The findings indicated that this algorithm effectively eliminated noise interference from partial discharge signals, thereby highlighting the original characteristics of these signals, which is beneficial for the maintenance of power equipment.

2. Theory

In VMD, the original signal is non-recursively decomposed into K subsequences, each characterized by distinct center frequencies and bandwidths. The objective of this decomposition process is to minimize the total bandwidth sum across all subsequences. The above problem could be transformed into a non-binding variational problem by introducing the augmented Lagrange function, and the optimal solution of Eq. (1) can be addressed [20].

$$\begin{cases} \min\left\{\sum_{k=1}^{K}\left\|\partial_t\left[(\delta(t)+\frac{j}{\pi t})*u_k(t)\right]e^{-j\omega_k t}\right\|_2^2\right\}, \\ s.t.\sum_{k=1}^{K}u_k=f(t). \end{cases} \tag{1}$$

Where $f(t)$ was the original signal; u_k was the k-th subsequence; ω_k was the center frequency of each subsequence; $\delta(t)$ was Dirac distribution role; ∂_t was gradient value at a given time t; $*$ was the convolution.

The Dung Beetle Optimizer (DBO) algorithm's merits included great optimization efficiency and fast convergence performance; nevertheless, its drawbacks included an imbalance between local development capability and global exploration, making it simple to slip into the local ideal scenario [21,22]. To address the issue of global optimization, an improved sine-based guidance mechanism was added to the dung beetle optimization technique, known as the MSADBO algorithm, which is an optimized DBO algorithm [23]. To address the aforementioned

imbalance in MSADBO, the Bernoulli chaotic mapping strategy, the enhanced sinusoidal algorithm strategy, and the adaptive Gauss-Cauchy mixed variation disturbance strategy were implemented. The signal was decomposed based on the VMD algorithm, and the parameters were optimized based on the DBO algorithm. The combined use of the two could optimize the key parameters of the VMD algorithm, thereby enhancing its decomposition performance.

Original population set's unpredictability was increased by the application of the Bernoulli chaotic mapping approach. Eq. (2) demonstrated the Bernoulli chaotic mapping technique [23]:

$$z_{n+1} = \begin{cases} \dfrac{z_n}{1-\beta}, & 0 \le z_n \le 1-\beta \\ \dfrac{z_n-(1-\beta)}{\beta}, & 1-\beta \le z_n \le 1 \end{cases} \tag{2}$$

Where β was the mapping parameter.

Improved sinusoidal algorithm (MSA) was introduced to coordinate the capacity for both local development and global exploration. It promoted the rapid dissemination of information in the population through information exchange with the current optimal individuals. The lack of information exchange among individuals in the original algorithm was changed. During the ball-rolling stage, MSA was used to modify the dung beetle placements, and improved locations updates were shown in Eq. (3) [23]:

$$x_i(i+1) = \begin{cases} x_i(i) + a \times k \times x_i(i-1) + b \times \Delta x, & \delta < ST \\ \omega_i x_i(i) + r_1 \times \sin(r_2) \times [r_3 p_i(i) - x_i(i)], & \delta \ge ST \end{cases} \tag{3}$$

Where $\delta = rand(1)$, $ST \in (0.5,1]$. ω_i was the coefficient of inertia. r_1 was a nonlinear decreasing function, r_2 was a random number on the interval $[0, 2\pi]$, and r_3 was a random number on the interval [-2, 2]. When $\delta < ST$ indicated that the dung beetles were in the typical stage of worldwide exploration and rolled with a purpose; when $\delta \ge ST$ indicated that dung beetles did not have a clear rolling goal but searched and moved through a sinusoidal function.

Equations (4), (5), and (6) displayed the most recent positions of the breeding dung beetles, juvenile dung beetles, and thieving dung beetles [23]:

$$B_i(t+1) = X^* + b_1 \times (B_i(t) - Lb^*) + b_2 \times (B_i(t) - Ub^*) \tag{4}$$

$$x_i(t+1) = x_i(t) + C_1 \times (x_i(t) - Lb^b) + C_2 \times (x_i(t) - Ub^b) \tag{5}$$

$$x_i(t+1) = X^b + S \times g \times (\left| x_i(t) - X^* \right| + \left| x_i(t) - X^b \right|) \tag{6}$$

Where b_1 and b_2 were independent random vectors, C_1 was a random number that follows a normal distribution, C_2 was a random vector of (0,1), g was an independent random vector that follows a normal distribution, and S was a constant. t was the quantity of existing iterations; $x_i(t)$ was the position of the i dung beetle at the t iteration; $x_i(t) - X^b$ was utilized to replicate variations in light intensity; $B_i(t+1)$ was the position of individual iteration during the foraging process.

An adaptive disturbance strategy combining Gauss and Cauchy variations was implemented to increase the variety of dung beetle population and broaden search space during later stages of algorithm's iterations, thereby helping to avoid premature convergence to local minima. The optimal individual was disturbed, and the superior position was chosen to proceed to the subsequent stage iteration by comparing the position before and after its variation. Equation (7) demonstrated the adaptive Gauss-Cauchy mixed variation disturbance technique [23]:

$$H^{\mathrm{b}}(t) = X^{\mathrm{b}}(t) * (1 + \mu_1 * Gauss(\sigma) + \mu_2 * cauchy(\sigma)) \tag{7}$$

Where $X^b(t)$ was optimal position of individual X in the t iteration; $H^b(t)$ was position of $X^b(t)$ after Gauss-Cauchy mixed disturbance; $Gauss(\sigma)$ was Gaussian mutation operator; $cauchy(\sigma)$ was Cauchy mutation operator.

The purpose of the greedy rule was to ascertain that evaluation metric corresponding to the newly obtained position obtained after variation disturbance was better than that of the original position. The greed rule was shown in Eq. (8) [23].

$$X^b = \begin{cases} H^b(t), & \mathrm{f}\left[H^b(t) \right] < \mathrm{f}\left[X^b(t) \right] \\ X^b(t), & \mathrm{f}\left[H^b(t) \right] \geq \mathrm{f}\left[X^b(t) \right] \end{cases} \tag{8}$$

Wavelet packet denoising algorithm was a denoising method based on wavelet packet decomposition, and the signals of low frequency and high frequency could be subdivided and synthesized by multiple levels [24]. It was necessary to set a suitable threshold to remove the noise. The noise reduction signal was reconstructed by the processed signal through the inverse transformation of the wavelet packet transform. In this paper, the decomposition of noisy partial discharge signals were based on the VMD algorithm, while the wavelet packet denoising algorithm reduced the noise of the decomposed pure signals, further

improving the signal-to-noise ratio of the signals.

Pearson correlation coefficient R was introduced to better distinguish between noisy signals and pure signals in the modes obtained by VMD decomposition. The noisy partial discharge signal and IMF had a higher correlation coefficient, and the correlation was stronger with the noisy partial discharge signal. The Pearson correlation coefficient was shown in Eq. (9) [25]:

$$R = \frac{\sum_{i=1}^{n}(x_i - \bar{x})(y_i - \bar{y})}{\sqrt{\sum_{i=1}^{n}(x_i - \bar{x})^2}\sqrt{\sum_{i=1}^{n}(y_i - \bar{y})^2}} \tag{9}$$

Where x_i was the component of the decomposed mode; y_i was the noisy partial discharge signal.

The following were the precise steps taken by the optimized VMD algorithm:

(1) The noisy partial discharge signal was simulated based on MATLAB software;

(2) The MSADBO algorithm was used to determine the optimal mode K and the quadratic penalty factor α of VMD, with the envelope entropy serving as the fitness function;

(3) Noisy partial discharge signal was broken down using the ideal parameters, and IMFs were produced;

(4) Compute the Pearson correlation for each mode with the noisy PD signal, assessing both noisy and pure indicators;

(5) After reconstruction, the components were subjected to a wavelet packet-based filtering procedure to remove noise, yielding the final enhanced signal;

(6) The interference signals were removed and the pure signals were reconstructed.

3. Simulation signal analysis

Partial discharge signals often exhibited the characteristic of oscillation attenuation. The PD signal recorded on-site in the study was frequently simulated using both single-exponential and double-exponential theories of oscillation attenuation. Double-exponential attenuation of oscillations model was adopted to simulate PD signal. The analytical form of the analog PD signals was shown in Eq. (10) [17]:

$$y(t) = A_0(e^{-1.3(t-t_0)/\tau_0} - e^{-2.2(t-t_0)/\tau_0}) \times \sin(2\pi f_L t) \tag{10}$$

Where A_0 was the peak value of the PD waveform, which was set to 40mV; t_0 was the onset time of the PD waveform; τ_0 was the attenuation time; f_L was the frequency of attenuated oscillation, which was set to 3MHz; The sampling rate was 50MHz; The sampling point is 500. Figure 1 presented the waveform corresponding to the initial PD signal simulation.

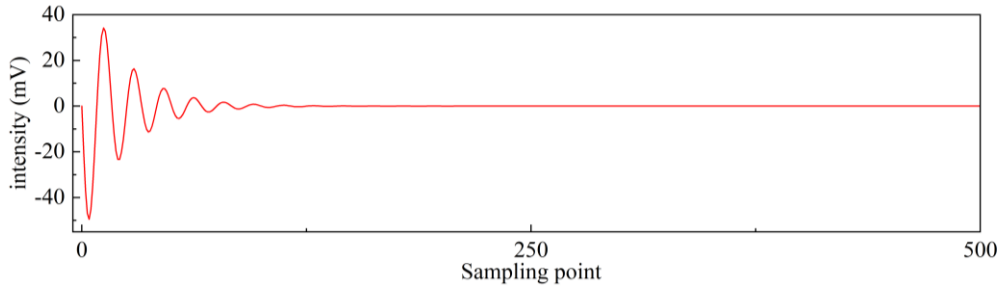

Fig. 1. The original simulation's partial discharge waveform

To replicate realistic interference conditions, a 5 dB white noise component was first superimposed onto the PD waveform, followed by two narrowband periodic disturbances-a 2 MHz sinusoid of 0.9 mV amplitude and a 6 MHz sinusoid of 2.5 mV amplitude. These periodic interferences, expressed as sine or cosine functions, are defined in Equation (11). The resulting noisy waveform is depicted in Figure 2.

$$S = A_i \sum_{i=1}^{n} \sin(2\pi f_i t) \tag{11}$$

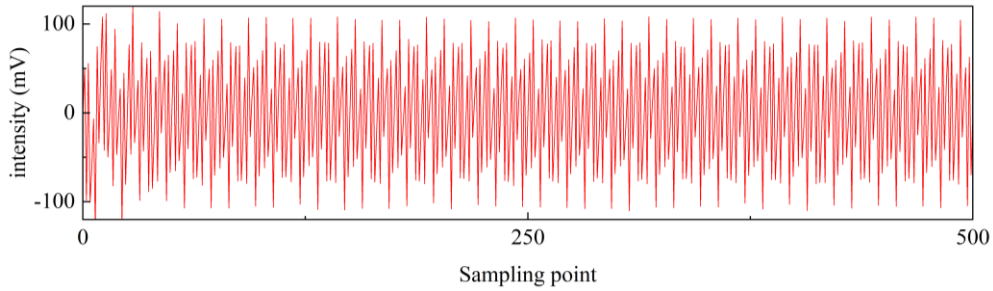

Fig. 2. The waveform of noisy PD signal

This value of K and α needed to be optimized before modal decomposition. The value range of K was [3,15], and the value range of α was [100,3000]. The fitness function was the minimal envelope entropy.

The maximum number of iterations was 20 and the population size was 30 in the MSADBO parameter settings. The fitness value reaches the minimum at the third iteration, and the parameter combination [K, α] were obtained as [7,1424].

Figure 3 illustrates that, over the course of the optimization iterations, the MSADBO algorithm achieved both rapid convergence and high precision, alongside reduced computation time and strengthened global search capability.

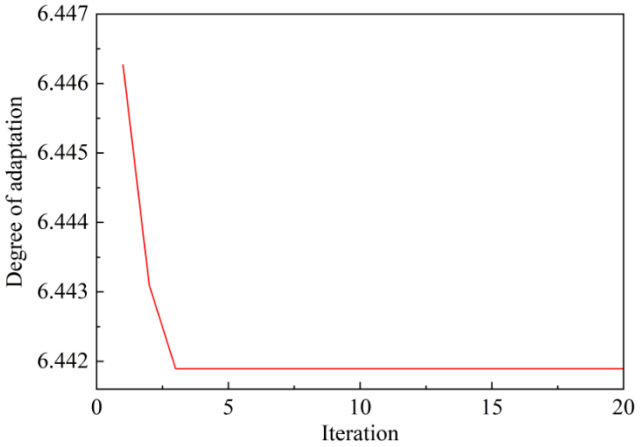

Fig. 3. The iterative curves of VMD optimized by MSADBO algorithm.

Once the VMD algorithm's ideal parameters were determined, the noisy partial discharge signal was broken down using the VMD algorithm. As shown in Fig. 4, the noisy partial discharge signal was decomposed into 7 IMF. The noisy partial discharge signal was completely decomposed based on the VMD algorithm. IMF3-IMF7 contained a large amount of noises, IMF1 contained a small amount of noise, and IMF2 was smooth and similar to the original partial discharge signal.

4. The noisy partial discharge signal and each IMF's Pearson correlation coefficients were computed using Eq. (9), as indicated in Table 1. Each IMF's similarity to the noisy partial discharge signal was assessed using the Pearson correlation coefficient. The component with a high Pearson correlation coefficient was the noisy component, while the opposite was the pure component. The Pearson correlation coefficient was defined as 0.9 in order to distinguish the noisy component from the pure component as much as possible. The Pearson correlation coefficient was calculated to be greater than 0.9, and IMF was the noisy component; otherwise, IMF was the pure component. The Pearson correlation coefficients calculated between IMF3-IMF7 and noisy partial discharge signal were greater than 0.9, which indicated that IMF3-IMF7 were noisy components and had a high similarity with the noisy partial discharge signal. The Pearson correlation coefficients calculated between IMF1 and IFM2 and the noisy partial discharge signal were less than 0.9, which indicated that IMF1 and IFM2 were pure components. As shown in Fig. 4, IMF3-IFM7 had a high similarity with noisy partial discharge signal, and IMF1 and IMF2 were almost different from noisy partial discharge signal, which verified the feasibility of setting the Pearson

correlation coefficient to 0.9.

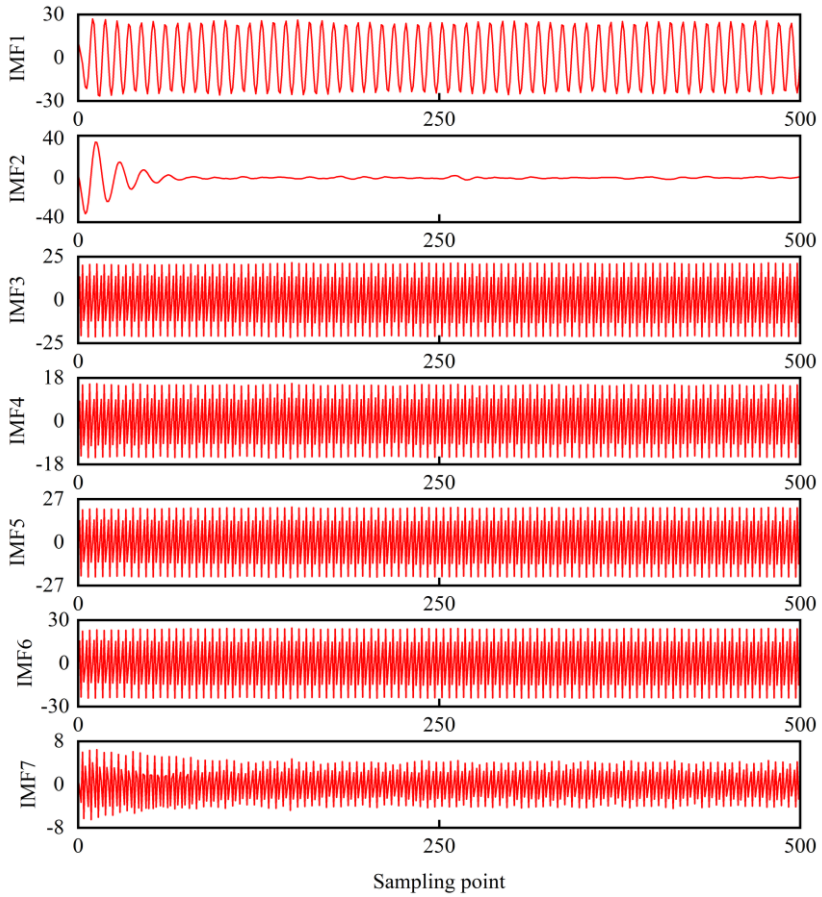

Fig. 4. IMFs were obtained after being decomposed by the VMD algorithm

Table 1

Correlation analysis was performed between the noisy partial discharge waveform and the decomposed IMFs

IMF	IMF1	IMF2	IMF3	IMF4	IMF5	IMF5	IMF7
R	0.0046	0.0028	0.9301	0.9289	0.9211	0.9130	0.9079

5. IMF3-IMF7 were eliminated, and IMF1 and IMF2 were reconstructed. To enhance signal clarity, the reconstructed waveform underwent denoising through the application of a wavelet packet-based algorithm, effectively suppressing noise components. Six decomposition layers were used, and "dB8" was chosen as the wavelet basis function. The decomposed wavelet coefficients were analyzed based on the default threshold method. After applying the wavelet packet denoising algorithm, the signal underwent noise reduction, resulting in the final denoised output.

6. Denoising effect of the algorithm was evaluated by the noise rejection ratio (NRR), and NRR was shown in Eq. (12).

$$\rho_{NRR} = 10(\lg \delta_1^2 - \lg \delta_2^2) \tag{12}$$

7. Where δ_1 was the signal's standard deviation was measured prior to the application of the noise reduction process; δ_2 was the standard deviation of the processed signal was computed to evaluate its stability following the noise reduction process. The larger the NRR, the higher the noise reduction rate.

8. Enhanced VMD method was used to remove noise from partial discharge signal. To evaluate its performance, a comparative analysis was conducted against both the EMD and the original VMD methods. As presented in Table 2, the Noise Reduction Ratio (NRR) achieved by the improved VMD algorithm exceeded those obtained by the EMD and standard VMD approaches, demonstrating its superior denoising capability. Meanwhile, when denoising the same partial discharge signal in a single run, the improved VMD algorithm exhibited a running time comparable to those of the EMD and VMD algorithms, which could fully meet the measurement requirements. Furthermore, as illustrated in Fig.5, the enhanced algorithm exhibited a more effective suppression of noise, resulting in a clearer and more refined signal. Overall, the reconstructed waveform obtained through the improved VMD method more accurately restored the original features of the partial discharge signal.

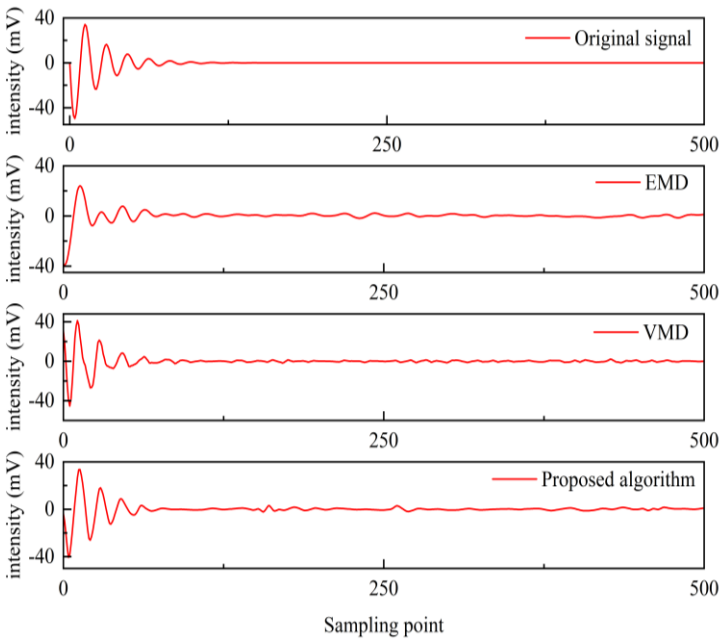

Fig. 5. Different algorithms were assessed and compared in terms of their ability to reduce noise

Table 2

Evaluation and Comparison of Multiple Algorithms

Comparison algorithm	EMD	VMD	Proposed algorithm
NRR(dB)	26.0703	27.4995	27.9841
Running time(s)	5.63	5.60	5.64

9. Conclusion

This study focused on the detection of partial discharge signals in electrical equipment, aiming to effectively suppress noise interference and accurately extract the characteristics of the original signals. After a series of experiments and analyses, the following key conclusions were obtained:

(1) The proposed improved VMD algorithm innovatively combined the MSADBO algorithm, VMD algorithm and wavelet packet denoising algorithm. The improved VMD algorithm had a higher NRR and offered better noise reduction performance, which could extract the characteristics of the original partial discharge signal more effectively versus EMD and VMD methods.

(2) This improved VMD algorithm had broad application prospects in the field of noise reduction of partial discharge signals and provided more reliable technical support for the accurate detection and fault diagnosis of partial discharge signals of electrical equipment.

Acknowledgments

This research has received funding from the Scientific and Technological lnnovation Project of lnner Mongolia Jingneng Kangbashi Thermal Power Co., Ltd. (Grant Nos. 1090JG2505).

R E F E R E N C E S

[1]. Thuc VC, Lee HS. Partial discharge (PD) signal detection and isolation on high voltage equipment using improved complete EEMD method. Energies. 2022 Aug 11;15(16):5819.

[2]. Govindarajan S, Natarajan M, Ardila-Rey JA, Venkatraman S. Partial discharge location identification using permutation entropy based instantaneous energy features. IEEE Transactions on Instrumentation and Measurement. 2021 Oct 19;70:1-2.

[3]. Yang X, Huang H, Shu Q, Zhang D, Chen B. Partial discharge signal extraction method based on EDSSV and low rank RBF neural network. IEEE Access. 2021 Jan 5;9:9744-52.

[4]. Hussain MR, Refaat SS, Abu-Rub H. Overview and partial discharge analysis of power transformers: A literature review. Ieee Access. 2021 Apr 23;9:64587-605.

[5]. Li L, Wei X. Suppression method of partial discharge interferences based on singular value decomposition and improved empirical mode decomposition. Energies. 2021 Dec 20;14(24):8579.

[6]. Yang J, Yan K, Wang Z, Zheng X. A novel denoising method for partial discharge signal based on improved variational mode decomposition. Energies. 2022 Nov 2;15(21):8167.

[7]. Huang NE, Shen Z, Long SR, Wu MC, Shih HH, Zheng Q, Yen NC, Tung CC, Liu HH. The empirical mode decomposition and the Hilbert spectrum for nonlinear and non-stationary

time series analysis. Proceedings of the Royal Society of London. Series A: mathematical, physical and engineering sciences. 1998 Mar 8;454(1971):903-95.
[8]. Ali M, Khan DM, Alshanbari HM, El-Bagoury AA. Prediction of complex stock market data using an improved hybrid emd-lstm model. Applied Sciences. 2023 Jan 21;13(3):1429.
[9]. Fang T, Zheng C, Wang D. Forecasting the crude oil prices with an EMD-ISBM-FNN model. Energy. 2023 Jan 15;263:125407.
[10]. Zeng F, Li L, Yang G, Sun M, Gong Q. Type identification of partial discharge signal based on emd decomposition and gwo-svm. In2021 China Automation Congress (CAC) 2021 Oct 22 (pp. 1476-1481). IEEE.
[11]. Dhandapani R, Mitiche I, McMeekin S, Mallela VS, Morison G. Enhanced partial discharge signal denoising using dispersion entropy optimized variational mode decomposition. Entropy. 2021 Nov 25;23(12):1567.
[12]. Jian L, Wang X, Huang S, Hao H, Zhang X, Yang X. Comparative analysis of different empirical mode decomposition-kind algorithms on sea-level inversion by GNSS-MR. Journal of Applied Geodesy. 2024 Jan 26;18(1):133-52.
[13]. Ahmadi F, Tohidi M, Sadrianzade M. Streamflow prediction using a hybrid methodology based on variational mode decomposition (VMD) and machine learning approaches. Applied Water Science. 2023 Jun;13(6):135.
[14]. Dragomiretskiy K, Zosso D., Variational mode decomposition. IEEE T Signal Proces 62 (3): 531–544 [Internet]. 2014
[15]. Cui H, Guan Y, Chen H. Rolling element fault diagnosis based on VMD and sensitivity MCKD. IEEE Access. 2021 Aug 30;9:120297-308.
[16]. Seyrek P, Şener B, Özbayoğlu AM, Ünver HÖ. An evaluation study of EMD, EEMD, and VMD for chatter detection in milling. Procedia Computer Science. 2022 Jan 1;200:160-74.
[17]. Lei Z, Wang F, Li C. A denoising method of partial discharge signal based on improved SVD-VMD. IEEE Transactions on Dielectrics and Electrical Insulation. 2023 Apr 24;30(5):2107-16.
[18]. Wu Z, Zhang Z, Zheng L, Yan T, Tang C. The denoising method for transformer partial discharge based on the whale VMD algorithm combined with adaptive filtering and wavelet thresholding. Sensors. 2023 Sep 26;23(19):8085.
[19]. Qi G, Zhao Z, Zhang R, Wang J, Li M, Shi X, Wang H. Optimized VMD algorithm for signal noise reduction based on TDLAS. Journal of Quantitative Spectroscopy and Radiative Transfer. 2024 Jan 1;312:108807.
[20]. Jiang Z, **e J, Zhang J, Zhang X. Denoising method of pipeline leakage signal based on VMD and Hilbert transform. Journal of Sensors. 2023;2023(1):1939606.
[21]. Zhang D, Wang Z, Zhao Y, Sun F. Multi-Strategy Fusion Improved Dung Beetle Optimization Algorithm and Engineering Design Application. IEEE Access. 2024 Jun 3.
[22]. He J, Guo W, Wang S, Chen H, Guo X, Li S. Application of Multi-Strategy Based Improved DBO Algorithm in Optimal Scheduling of Reservoir Groups. Water Resources Management. 2024 Apr;38(6):1883-901.
[23]. J. Pan, S. Li, P. Zhou, g. Yang, and D. Lv, Dung beetle optimization algorithm guided by improved sine algorithm, Computer Engineering and Applications, 2023.
[24]. Liu K, Yin G, Zhang Z, Yang P, Lu H, Li D, Zhu T. High-resolution and high-precision φ-OFDR strain sensing scheme based on adaptive phase unwrap** and wavelet packet denoising. Journal of Lightwave Technology. 2024 Jan 15;42(2):891-7.
[25]. Pan Z, Xu D, Zhang Y, Wang M, Wang Z, Yu J, Zhang G. New energy transmission line fault location method based on Pearson correlation coefficient. Journal of Physics: Conference Series 2024 Mar 1 (Vol. 2717, No. 1, p. 012007). IOP Publishing.